IL NUOVO CIMENTO **48 C** (2025) 179
DOI 10.1393/ncc/i2025-25179-9

COMMUNICATIONS: SIF Congress 2024

A workflow for forward and inverse modelling of ground deformations associated with pre-eruptive magma ascent scenarios

A. SPINA

Department of Physics and Astronomy, Alma Mater Studiorum, University of Bologna Bologna, Italy

received 30 January 2025

Summary. — Volcanic eruptions are often preceded by geophysical signals such as ground deformation and seismicity. These signals are frequently combined with information from previous unrest and eruption episodes and physical models to explore possible scenarios for the future behavior of the volcanic system. This task is especially challenging for volcanoes that have not erupted in recent decades: scarce data on their behavior necessarily lead to poorly constrained scenarios. This study proposes a workflow for defining physics-based magma ascent scenarios, leveraging on the physical understanding of magmatic unrest gained at volcanoes worldwide. The proposed workflow involves several steps: constraining the stress field, simulating dike ascent with a 3D numerical model, calculating the induced surface deformation and using the simulated data to verify our ability to track magma ascent as various processes complicate the unrest. I illustrate the workflow with a synthetic example and discuss how to further develop this approach.

1. – Introduction

Some of the largest eruptions on Earth, with volumes of up to a few hundred km^3, are hosted by calderas; these eruptions are highly destructive natural hazards, capable of devastating large areas and altering the climate for decades [1]. Some active calderas, such as Campi Flegrei (CF) in Italy, are densely populated. Calderas also tend to erupt infrequently —*e.g.*, at CF the last eruption occurred in 1538 [2], so that we lack data and, as a consequence, they are poorly understood systems. In these cases, numerical modeling may help clarify the dynamics of the magmatic system during restless times and pre-eruptive magma run-up phases. This may also be useful in assessing the volcanic hazards.

Calderas are defined by large, approximately circular depressions formed by the collapse of the reservoir roof following a large eruption. They often exhibit complex inner structures, with shallow or deep sediment infill often consisting of ignimbrites from past eruptions, large hydrothermal systems, several rings of faults associated with collapse events, resurgent domes, and voluminous, long-lived magmatic systems [3]. Currently,

about 100 of the 446 known calderas on Earth are in a state of "unrest" [4], meaning that the recorded ground deformation, degassing, seismicity and gravity changes are "out of the ordinary" for the specific volcano. Unrest at volcanoes is linked to a heightened probability of eruption within months [5, 6], although the relationship between specific patterns in the monitoring data and the likelihood of eruptions are still unclear. In particular, heightened levels of activity are often attributed to pressurisation due to supply of melt or other fluids; one of the challenges is to tell magmatic and hydrothermal processes apart during an unrest phase [7], since hydrothermal deformation can hide the —usually weaker— deformation caused by magma accumulation.

An effective way to interpret geophysical signals at volcanoes is to compare observations with the expected signals calculated through mathematical models for the pressurization or migration of magma and other fluids. Ground deformation is a key monitoring technique to understand volcanic processes and to forecast eruptions.

Magma is transported through the brittle-elastic crust via a process called diking, which is a mechanism analogous to hydraulic fracturing. Dikes are thin, predominantly tensile fractures filled with magma [8]. They may be generated deep in the Earth's lithosphere or at shallow levels due to injection from a melt reservoir. Once they are formed, dikes propagate by fracturing the host rock. The formation and propagation of dikes produce deformation patterns that can be anticipated and used to infer the presence and geometry of such intrusions. These patterns are generated by the dilation of the surrounding rock as the fracture walls are forced apart.

Campi Flegrei's deformation is well-monitored: the caldera hosts 25 GNSS stations, and InSAR interferograms are routinely analysed to track the deformation due to the underground pressurization [9]. By retrieving the optimal deformation source parameters, including depth, shape and volume change, we can pinpoint the type of causative source. Shapes like spheres or ellipsoids [10-12] act as simple models of magma chambers, while thin cracks [13, 14] represent tabular intrusions. Triaxial source models, the Compound Dislocation Model [15], and the finite Ellipsoidal Cavity Model [16], can be used to infer the deformation source parameters without prior assumptions on the shape of the source.

The above models describe the deformation induced by volume changes within elastic host rocks but do not describe the dynamics of magma ascent. Modelling magma propagation is challenging because it involves the coupling of elasticity in the host rock, fluid dynamics in the interior of the crack, fracture mechanics at the propagating tip, and, in general, phase transitions and heat transport, all occurring within the moving dike walls. The propagation of large dikes filled with low-viscosity magmas may be simplified by assuming magma as an inviscid fluid, which drastically simplifies the fluid dynamic problem, so that the energetically preferred trajectory of the dike can be calculated [17-19]. The downside is that by neglecting the viscous flow the information on the timing of the process is lost, and dike velocity needs to be estimated with a different approach.

Since dikes are predominantly opening cracks, their energetically preferred orientation is roughly perpendicular to the least compressive principal stress axis. Accurately replicating observed deformation patterns thus requires not only modeling the dike geometry, but also incorporating the background stress field that controls dike trajectory and orientation. However, the stress field is difficult to constrain, particularly in complex caldera systems like CF, where it is still poorly defined. Furthermore, hydrothermal systems complicate both deformation signals and mechanical behavior, influencing dike propagation and interpretation.

Previous studies have defined and tested workflows to simulate magma propagation beneath a caldera [20, 21]. I build on these studies to propose additional steps for estimating geophysical observables associated with magma ascent toward the surface. This workflow can be adapted to forecast eruption scenarios once the stress field of the specific volcanic system has been accurately calibrated [20, 22].

In the following, I outline the physical principles underlying this approach and apply it to a simplified synthetic scenario, loosely inspired by the CF caldera setting.

2. – Simulation of a pre-eruptive magma propagation scenario

I propose a general procedure composed of the following steps: 1) Simulate the stress field required as input to the 3D dike propagation model; 2) Set other input parameters and run dike simulations with the Three-dimensional Intrusion Model (TIM); 3) Simulate the deformations expected at fixed GNSS stations as the dike ascends; 4) Invert the simulated ground displacements to find the location and the size of the best-fitting deformation source.

2˙1. *Stress model.* – Regional stress and gravitational loading are usually the dominant sources of stress at volcanoes [22]. In a Cartesian reference frame with z positive upward, I consider a weakly tensional regional stress, as appropriate for CF [22] with $\sigma_{xx} = 4$ MPa, $\sigma_{yy} = 2$ MPa, $\sigma_{xy} = 0$ MPa (tensile stresses are positive). I also consider gravitational loading stresses due to the presence of a caldera and a hill (fig. 1(a)). I use two analytical functions to reproduce the stress induced by these topographic features, assuming a distribution of point forces scaled according to the topography. To approximate the caldera unloading, I use the "bump" function

$$f_c = \begin{cases} \frac{d}{e^{-1}} \exp\left[-\frac{R_c^2}{r_c^2 - R_c^2}\right], & \text{if } r_c^2 < R_c^2, \\ 0, & \text{if } r_c^2 \geq R_c^2, \end{cases} \tag{1}$$

where $r_c = \sqrt{(x - X0_c)^2 + (y - Y0_c)^2}$, d is the caldera depth set to 400 m; R_c is the caldera radius set to 7.5 km; and $X0_c = 0$ km, $Y0_c = 0$ km are the coordinates of the caldera center. To approximate the gravitational loading due to the hill, I use a Gaussian function

$$f_h = h \cdot \exp\left[-\frac{r_h^2}{2R_h^2}\right], \tag{2}$$

where $r_h = \sqrt{(x - X0_h)^2 + (y - Y0_h)^2}$, h is the hill height set at 150 m; R_h is the hill radius fixed at 1.5 km, $X0_h = 7$ km, $Y0_h = 7$ km are the coordinates of the hill's center.

In fig. 1(c) and fig. 1(d), the red vectors show the stress field on a $x - y$ cross-section through the center of the caldera (fig. 1(b)). Given that dikes tend to align perpendicular to the direction of the least principal stress, *e.g.*, [17], the stress field induced in the subsurface by the loading/unloading due to the hill and caldera drives ascending dikes to turn horizontal, with dikes becoming progressively steeper as they propagate laterally away from the caldera axis. Consequently, in the case considered here, the dikes will be deflected by the caldera and attracted by the hill, as shown below.

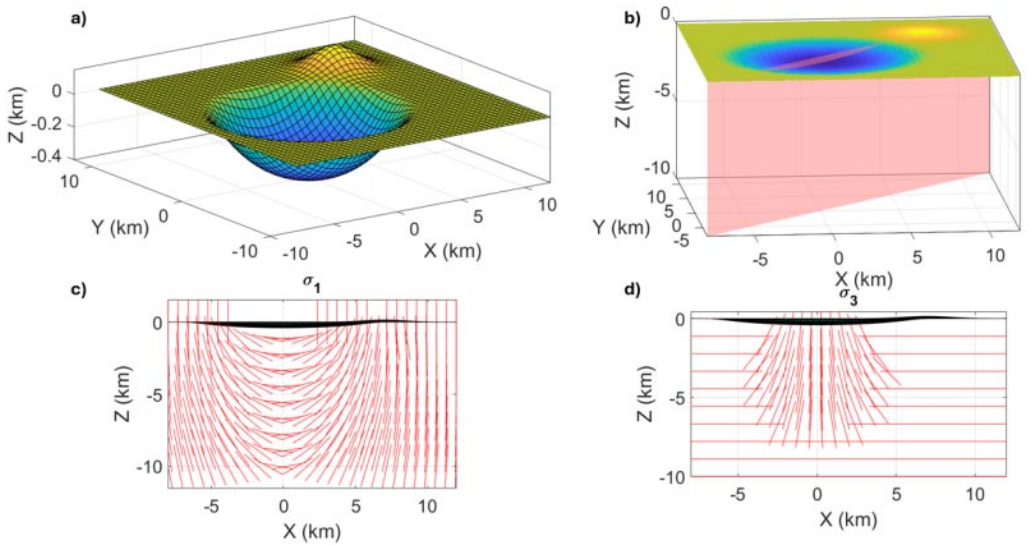

Fig. 1. – (a) Three-dimensional representation of the synthetic topography, where the caldera and the hill are highlighted. (b) Representation of the topography, featuring the caldera (in blue) and the hill (in yellow). The diagonal cross-section is shown in red. (c) and (d): the direction of the most (σ_1) and least (σ_3) compressive principal stress axes across the section shown in (b). The topographic profile is represented in black with the caldera centered in $x = 0$ km and the hill centered at $x = 7$ km and $y = 7$ km.

2˙2. *Simulation of dike ascent and induced ground deformation.* – To simulate the dike ascent, I use a fully 3D model to calculate the evolving 3D shape of a dike that can bend and twist with full degrees of freedom [19]. The dike is represented as a Boundary Element fracture, discretized with triangular dislocations [23]. To initialize the model, it is necessary to define the starting configuration. In particular, at CF caldera [2] and at many other calderas [22], dikes nucleate from a sill-shaped magma storage; thus, I initialize the dike as a slightly off-centered sub-horizontal penny-shaped crack (table I).

The dike takes an oblique trajectory that becomes progressively steeper (fig. 2(a)). The dike shape, given the choice of the parameters (table I), does not change much over the course of propagation. Dike shape changes would be expected if, *e.g.*, the density difference between host rock and dike changed during propagation. After ascending obliquely, the dike is expected to erupt outside the caldera. The code run was stopped at ~ 500 m below the surface.

TABLE I. – *TIM input parameters. X_s, Y_s and Z_s are the coordinates of the starting dike center, V_C is the dike volume, μ is the shear modulus, ν is the Poisson ratio and K_C is the rock's fracture toughness.*

TIM run parameters									
X_s (km)	Y_s (km)	Z_s (km)	V_C (m^3)	Dip (°)	Strike (°)	μ (Pa)	ν	ρ_m (kg/m^3)	K_C ($Pa\cdot\sqrt{m}$)
0.5	0	−3.5	$12 \cdot 10^6$	18	45	$6 \cdot 10^9$	0.25	2200	$2 \cdot 10^8$

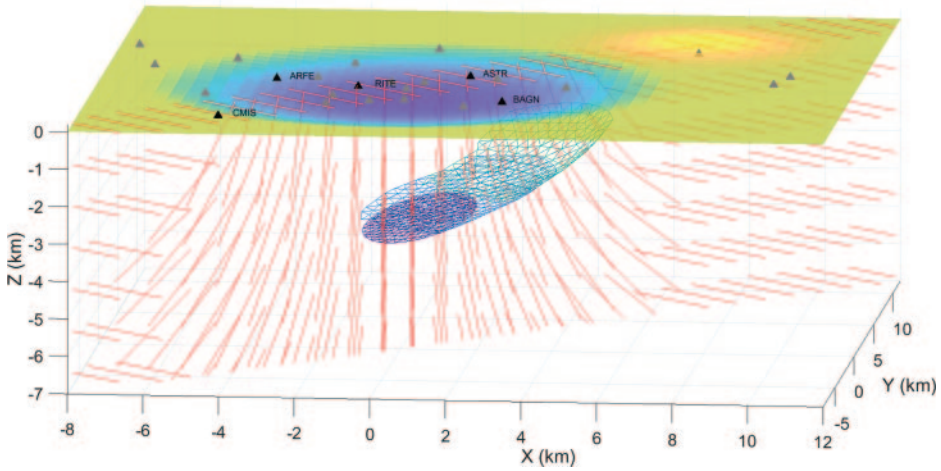

Fig. 2. – Perspective view of the propagating dike within the external stress field. The red segments represent the σ_3 direction. The caldera floor is illustrated in blue, and the hill is depicted in yellow. The triangles (in grey and black) indicate the locations of GNSS stations, with particular emphasis on the following stations (in black): ARFE (Arco Felice), ASTR (Astroni), BAGN (Città della Scienza Bagnoli), CMIS (Capo Miseno), RITE (Rione Terra).

For each step of the simulated propagation, TIM outputs the tensile-slip, strike-slip, and dip-slip for all dislocations composing the mesh. By using this information, I simulate the deformations expected at GNSS stations as the dike ascends. For this purpose, I use the MatLab functions in [23] to calculate the displacements associated with triangular dislocations (TDs) in a homogeneous elastic half-space. I obtain the total displacements in East, North, and vertical directions by summing all the displacements calculated on the surface due to each TDs. Then I add a Gaussian noise of 2 mm in the horizontal direction and 5 mm in the vertical direction to simulate displacement errors expected at the GNSS stations (fig. 2).

2˙3. *Inversion of ground deformation.* – I invert the simulated noisy displacements for three snapshots of the simulated dike trajectory (fig. 2) using the Compound Dislocation Model (CDM) by [16], combined with the Genetic Algorithm MatLab function, to find the best-fitting deformation source's location and size (table II). In all the inversions, I use as objective function the sum of squares of the residuals.

The inversions are successful in recovering the dike's volume and position (fig. 3(a)), as confirmed by comparing the inverted parameters (table II) with those provided as input (table I). In particular, the volume of the dike, calculated as

$$\Delta V = 4 \cdot \Delta u (a_x \cdot a_y + a_x \cdot a_z + a_y \cdot a_z), \tag{3}$$

where Δu is the dislocation opening and a_x, a_y, and a_z are the semi-axes of the rectangular dislocations that compose the CDM, is well recovered by the inversions. The inverted volumes error is $\sim 8\%$. The goodness of the inversion results can also be visually assessed by comparing the simulated and modeled displacements (fig. 3(c), (d) and (e)).

TABLE II. – *Inverted parameters for the three snapshots: d is depth, a_x, a_y, a_z the semi-axes, ω_X, ω_Y and ω_Z the rotation angles, and Δu is the opening.*

	Inverted parameters with CDM										
	X_0 (km)	Y_0 (km)	d (km)	a_x (m)	a_y (m)	a_z (m)	ω_x (°)	ω_y (°)	ω_z (°)	Δu (m)	ΔV (m^3)
1°	0.51	0.17	3.3	390.4	985	958.6	155.3	73.4	133.8	2	$1.3 \cdot 10^7$
2°	2	1.4	3.1	324.2	992.7	984.9	164.8	252.4	150.7	1.9	$1.3 \cdot 10^7$
3°	3.2	2.2	1.7	361.1	842.1	979	232.4	218.6	131.9	1.9	$1.1 \cdot 10^7$

3. – Discussions and conclusions

This work represents a first step towards setting up procedures to define magma ascent scenarios. The procedure can be easily generalized to natural volcanic settings, provided the stress field is well-constrained.

The procedure I adopted presents several limitations, some of which are inherent in the model employed for simulating magma transport, while others are a consequence of the inversion procedure. The stress field I simulated is very simple and is still too rough to properly approximate the CF caldera structure. I did not consider the real topography of CF, the presence of sediments inside the caldera, the presence of faults and/or pre-

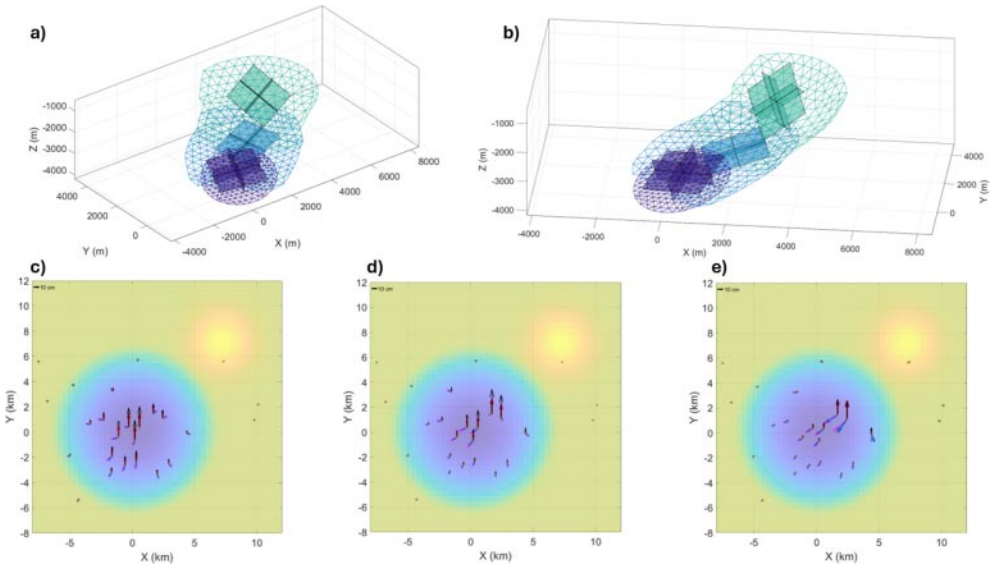

Fig. 3. – (a) The inversion with CDM for the three snapshots of the simulated propagating dike. (b), (c), (d): red and blue vectors are vertical and horizontal component of the simulated displacements, while black and pink vectors are vertical and horizontal components of the displacements relative to the best-fit parameters for the three snapshots in panel (a). The "+" symbols in green are the GNSS stations.

existing intrusions, and the hydrothermal system. To achieve a better constraint of the stress field, one way would be to follow the method of [22] and [24]. Moreover, I neglected changes in magma density throughout propagation. However, I note that the shape of the dikes I obtain from the simulations has general value: by changing the stress field, the trajectory and the orientation of the dike (strike, dip) will change but the shape of the dike will not change substantially, unless the density profile in the host rocks is modified, which would lead the dike to expand sideways rather than propagating straight up.

I used a uniform Poisson's ratio and shear modulus for the entire half-space, since layers of different elastic parameters cannot currently be modeled by TIM.

An important aspect is the density layering, *i.e.,* variations in density in the Earth's crust. The density of rock (ρ_r) and magma (ρ_m) are functions of depth and, for magma, time as well. The difference between ρ_r and ρ_m has large influence on the propagation of a dike and chances of getting arrested on the way. Furthermore, the density of the magma can influence the trajectory, as it contributes to the dike's buoyancy pressure and, thus, to how closely dikes follow trajectories dictated by principal stress axes [25, 26]. Here, I consider the rock and magma density constant and uniform during the propagation, to reduce the complexity of the problem.

For a meaningful application to CF, it is important to calculate a more realistic ground deformation; indeed, the hydrothermal system is expected to contribute to the observed surface displacements. To improve our understanding of the interpretation of deformation measurements and develop approaches for magma ascent early warning, it is necessary to be able to distinguish the deformations due to the ascent of the magma from those due to the pressurization of the hydrothermal system.

In conclusion, the workflow presented here is a first step to developing a general method for calculating magma ascent scenarios. In spite of the many simplifications, this work shows that simulating the geophysical observables induced by magma ascent is feasible with the current state of the art. The proposed workflow can be generalized to more complex scenarios through building on previous work [19, 20, 23]. Future works can focus on better defining the stress field [24] and exploring variations in the input parameters to TIM, such as volume, density, depth etc. Refining the model to enhance its realism and improving its application to CF will contribute to advance our understanding of magma migration at calderas. Moreover, by helping quantify critical parameters linked to pre-eruptive magma migration, this model may provide crucial support for activities such as developing effective risk mitigation strategies.

* * *

I wish to express my gratitude to the anonymous Reviewer, whose constructive remarks and suggestions have considerably improved the quality of the present work. I also wish to thank E. Rivalta, M. Nikkhoo and L. Mantiloni for the useful insights and precious advice.

REFERENCES

[1] Acocella V. *et al.*, *Rev. Geophys.*, **53** (2015) 896.
[2] Di Vito *et al.*, *Sci. Rep.*, **6** (2016) 32245.
[3] Acocella V., *Earth Sci. Rev.*, **85** (2007) 125.
[4] Bevilacqua A. *et al.*, *Volcanic Hazard Assessment at the Campi Flegrei Caldera, Italy*, in *Campi Flegrei: A Restless Caldera In A Densely Populated Area* (Springer, Berlin, Heidelberg) 2022.

[5] Phillipson G. *et al.*, *J. Volcanol. Geoth. Res.*, **264** (2013) 183.
[6] Sandri L. *et al.*, *Geochem. Geophys. Geosyst.*, **18** (2017) 2748.
[7] Scaillet, Bruno *et al.*, *Nat. Geosci.*, **18** (2025) 115.
[8] Rubin A., *Annu. Rev. Earth Planet. Sci.*, **23** (1995) 287.
[9] Giudicepietro F. *et al.*, *Int. J. Appl. Earth Observ. Geoinf.*, **132** (2024) 104060.
[10] Mogi K., *Bull. Earthq. Res. Inst.*, **36** (1958) 99.
[11] McTigue D., *J. Geophys. Res.: Solid Earth*, **92** (1987) 12931.
[12] Yang X. *et al.*, *J. Geophys. Res.: Solid Earth*, **93** (1988) 4249.
[13] Okada Y., *Bull. Seismol. Soc. Am.*, **75** (1985) 1135.
[14] Fialko Y. *et al.*, *Geophys. J. Int.*, **146** (2001) 191.
[15] Nikkhoo M. *et al.*, *Geophys. J. Int.*, **208** (2017) 877.
[16] Nikkhoo M. *et al.*, *Geophys. J. Int.*, **232** (2023) 643.
[17] Dahm T., *Geophys. J. Int.*, **141** (2000) 623.
[18] Maccaferri F. *et al.*, *Geophys. J. Int.*, **180** (2010) 1107.
[19] Davis T. *et al.*, *Geophys. Res. Lett.*, **47** (2020) e2020GL087774.
[20] Mantiloni L. *et al.*, *J. Geophys. Res.: Solid Earth*, **128** (2023) e2022JB025956.
[21] Davis T. *et al.*, *Geophys. Res. Lett.*, **48** (2021) e2021GL093038.
[22] Rivalta E. *et al.*, *Sci. Adv.*, **5** (2019) eaau9784.
[23] Nikkhoo M. *et al.*, *Geophys. J. Int.*, **201** (2015) 1119.
[24] Mantiloni L. *et al.*, *J. Geophys. Res.: Solid Earth*, **129** (2024) e2023JB028409.
[25] Watanabe T. *et al.*, *Earth Planets Space*, **54** (2002) e1247.
[26] Maccaferri F. *et al.*, *Geochem. Geophys. Geosys.*, **20** (2019) 2064.